A new probe of magnetic fields in the pre-reionization epoch: II. Detectability

Vera Gluscevic,[1] Tejaswi Venumadhav,[1] Abhilash Mishra,[2] Antonija Oklopcic,[2] and Christopher Hirata[3]

[1] *Institute for Advanced Study, Einstein Drive, Princeton, NJ 08540, USA*
[2] *California Institute of Technology, Mail Code 350-17, Pasadena, CA 91125, USA*
[3] *Center for Cosmology and Astroparticle Physics, The Ohio State University, 191 West Woodruff Lane, Columbus, Ohio 43210, USA*

(Dated: March 3, 2016)

In the first paper of this series, we proposed a novel method to detect large-scale intergalactic magnetic fields during the Dark Ages, using future 21-cm tomography surveys. In this paper, we examine detectability of magnetic fields using this method. We first develop a minimum-variance estimator formalism that relies on identifying the characteristic anisotropic imprints in the 21-cm brightness-temperature 2-point correlation functions. We then perform Fisher forecast for this estimator and find that a radio array consiting of a square kilometer of dipole antennas (such as the next-generation of HERA, and the SKA) can detect fields of strength on the order of 10^{-21} Gauss at redshifts of 20, reaching almost 10 orders of magnitude below the current CMB constraints.

I. INTRODUCTION

Magnetic fields are ubiquitous in the universe on all observed scales [? ? ? ? ?]. However, the origins of the magnetic fields in Galaxies and on large scales are as of yet an unresolved question. Various forms of dynamo mechanisms [?] are proposed to maintain and amplify magnetic fields, but they typically require seed fields to act [?]. The seed fields may be produced during structure formation through Biermann battery or similar mechanisms [? ?], or otherwise may be relics from the early universe [? ? ?]. Observations of large-scale weak magnetic fields in the high-redshift intergalactic medium (IGM) can thus provide tools for understanding the origins of magnetic fields in the present-day universe, and potentially open up an entirely new window into the physics of the early universe.

Many observational probes have previously been used to search for evidence of large-scale magnetic fields locally and at high redshifts; see, e. g. [? ? ? ? ? ? ? ? ? ? ?]. Amongst the most sensitive tracers of cosmological magnetic fields are the measurements of the cumulative effect of Faraday rotation in the cosmic-microwave-background polarization maps, which currently place an upper limit of $\sim 10^{-10}$ Gauss (in comoving units) using the data from the Planck sattelite [?]. In Paper I of this series [?], we proposed a novel method to detect and measure extremely weak cosmological magnetic fields during the pre-reionization epoch (the Dark Ages). This method relies on future 21-cm brightness-temperature tomography surveys [? ?], many of which have pathfinder experiments currently running [? ? ? ? ? ?], and plans for the next stages to be realized in the coming decade [? ?]. As we show in Paper I, the measurement of statistical anisotropy in the 21-cm signal from the Dark Ages has intrinsic sensitivity to magentic fields in the IGM more than *10 orders of magnitude below the current upper limits.*

While Paper I layed out the formalism necessary to account for the effect of magnetic fields on the statistics of the 21-cm signal, this paper (which we refer to as Paper II in the following) focuses on evaluating the sensitivity of future 21-cm experiments using this method. The rest of this paper is organized as follows. In §II, we present a quick overview of the main results in Paper I. In §IV, we derive minimum-variance estimators for a uniform and stochastic magnetic field. In §V, we set up the Fisher analysis formalism necessary to evaluate detectability. In §VI, we present numerical results, and we conclude in §VII. Supporting materials are presented in the appendicies.

II. SUMMARY OF THE METHOD

Magnetic moments of hydrogen atoms in the excited state of the 21-cm line transition tend to be aligned with the incident quadrupole of the 21-cm radiation from the surrounding medium. This effect of "ground-state alignment" [? ?] arises in a cosmological setting due to velocity-field gradients. In the presence of external large-scale magnetic fields, the emitted 21-cm quadrupole is misaligned with the incident quadrupole, due to atomic precession (illustrated in Figure 1). The resulting emission anisotropy can thus be used to trace magnetic fields at high redshifts.

The main result of Paper I was a calculation of the 21-cm brightness temperature T as a function of the line of sight direction $\widehat{\mathbf{n}}$, in the frame of the emitting ensamble of atoms. The relevant expression is

$$T(\widehat{\mathbf{n}},\widehat{\mathbf{k}}) = \left(1-\frac{T_\gamma}{T_\mathrm{s}}\right) x_{1\mathrm{s}} \left(\frac{1+z}{10}\right)^{1/2} \times\Bigg[26.4\ \mathrm{mK}\Big\{1+\left(1+(\widehat{\mathbf{k}}\cdot\widehat{\mathbf{n}})^2\right)\delta\Big\} - 0.128\ \mathrm{mK}\left(\frac{T_\gamma}{T_\mathrm{s}}\right) \times x_{1\mathrm{s}}\left(\frac{1+z}{10}\right)^{1/2}\Big\{1+2\left(1+(\widehat{\mathbf{k}}\cdot\widehat{\mathbf{n}})^2\right)\delta - \frac{\delta}{15}\sum_m \frac{4\pi}{5}\frac{Y_{2m}(\widehat{\mathbf{k}})\,[Y_{2m}(\widehat{\mathbf{n}})]^*}{1+x_{\alpha,(2)}+x_{\mathrm{c},(2)}-imx_\mathrm{B}}\Big\}\Bigg], \tag{1}$$

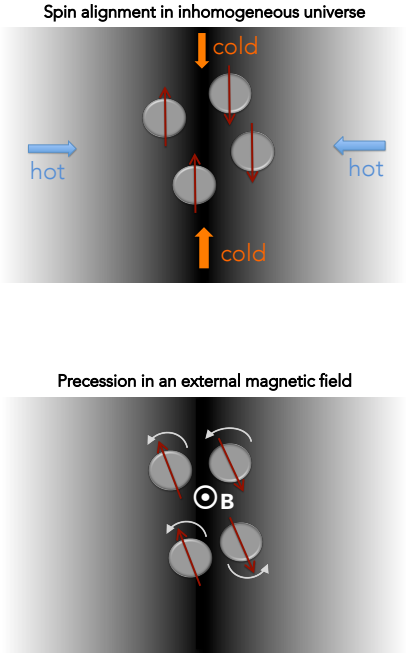

Figure 1. Illustration of the effect of a magnetic field on hydrogen atoms in the excited state of 21-cm transition at high redshifts. In the classical picture, magnetic moments of the atoms (depicted as red arrows) tend to be aligned with density gradients (upper panel; the gradient is depicted with the background shading), unless they precess about the direction of ambient magnetic field (pointing out of the page on the lower panel). When the precessing atoms decay back into the ground state, the emitted quadrupole (aligned with the direction of the magnetic moments) is misaligned with the incident quadrupole. This offset can be observed as a statistical anisotropy of 21-cm-brightness-temperature correlation functions, and used to trace cosmological magnetic fields.

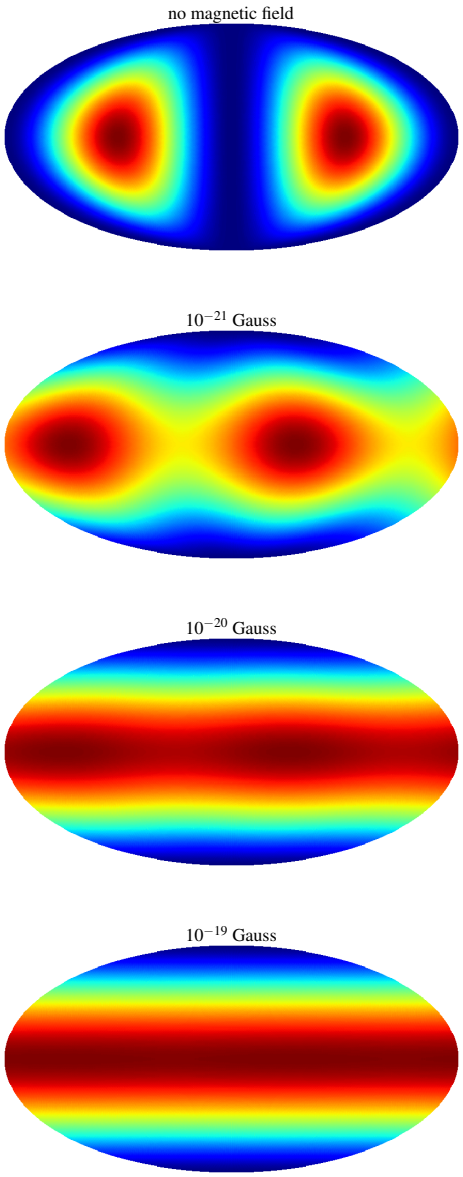

Figure 2. Illustration of the quadrupolar pattern of 21-cm emission from the last (B-dependent) term of Eq. (1) in the frame of the emitting atoms, for the case where $\vec{k}$ is perpendicular to $\widehat{\mathbf{n}}$ (maximal signal), shown in Molleweide projection. Lower panels correspond to increasingly stronger magnetic fields (strength denoted on each panel in comoving units), with the bottom panel corresponding to the saturated case. Notice how the type of quadrupole differs for the no-magnetic field case and the case the field is "strong" in the saturation sense.

where $x_{\alpha,(2)}$, $x_{c,(2)}$ and x_B parametrize the rates of depolarization of the ground state by optical pumping, collisions, and magnetic precession (relative to radiative depolarization), respectively (defined in detail in Paper I). Furthermore, T_s and T_γ are the spin temperature and the temperature of the cosmic microwave background at redshift z, respectively; $\widehat{\mathbf{k}}$ is a unit vector in the direction of the wave-vector $\vec{k}$ of a given density Fourier mode; and Y_{2m} represent the usual spin-zero spherical harmonics. Figure 2 illustrates the effect of the magnetic field on the brightness temperature emission pattern in the frame of the atom; shown are quadrupole patterns corresponding to the sum-term of Eq. (1), for various strengths of the magnetic field. Notice that there is a saturation limit for the field strength—for strong enough fields, the precession time is much smaller than the lifetime in the excited state, and when the emission pattern assymptotes to the one shown in the bottom panel of Figure 2. Above this limit, approximation of linear dependence of T breaks down, which implies that the signal cannot be used to reconstruct the strength of the field; however, it is still possible to distinguish saturated regime from the case of null field, as we will see in §V.

The affect of quadrupole misalignement arises at second order in optical depth (it is a result of a two-

scattering process), and is thus a small correction to the total brightness temperature. However, owing to the long lifetime of the excited state (during which even an extremely slow precession has large cumulative effect on the direction of the quadrupole at second order), the effect of misalignement is excuisitively sensitive to magnetic fields in the IGM at redshifts prior to cosmic reionization—as we show in Paper I, a miniscule magnetic field strength of 10^{-21} Gauss (in comoving units) produces order-one changes in the direction of the quadrupole. This means that a high-precision measurement of the 21-cm brightness-temperature 2-point correlation function intrinsically has that level of sensitivity to detecting magnetic fields in the Dark Ages. We now proceed to develop a formalism to search for this effect, with future surveys of redshifted 21-cm line, and to identifying experimental setups that can reach it.

III. BASICS

Before focusing on the estimator formalism in the next Section, here we review the basics of 21-cm brightness temperature fluctuation measurements. In §III A, we review definitions of quantities describing sensitivity of interferometric radio arrays; in §III B, we focus on the derivation of the noise power spectrum; and in §III C, we discuss the effects of the array configuration and its relation to coverage of modes in the uv plane of the array.

A. Definitions

The redshifted 21-cm signal can be represented as a specific intensity at the location in physical space $I(\vec{r})$, or in Fourier space $\widetilde{I}(\vec{k})$. In sky coordinates (centered on an emitting patch of the sky), these functions become $\mathcal{I}(\theta_x, \theta_y, \theta_\nu)$, and $\widetilde{\mathcal{I}}(u, v, \eta)$, respectively. Here, vector $\vec{k}$ (in the units of comoving Mpc^{-1}) is a Fourier dual of $\vec{r}$ (comoving Mpc), and likewise, θ_x (rad), θ_y (rad), and θ_ν (Hz) are duals of the coordinates u (rad^{-1}), v (rad^{-1}), and η (seconds), respectively. Notice that θ_x and θ_y represent the angular extent of the patch in the sky, while θ_ν represents its extent in the frequency space. The two sets of coordinates are related through linear transformations in the following way

$$\begin{aligned} \theta_x &= \frac{r_x}{\chi(z)}, & u &= \frac{k_x \chi(z)}{2\pi}, \\ \theta_y &= \frac{r_y}{\chi(z)}, & v &= \frac{k_y \chi(z)}{2\pi}, \\ \theta_\nu &= \frac{H(z)\nu_{21}}{c(1+z)^2} r_z, & \eta &= \frac{c(1+z)^2}{2\pi H(z)\nu_{21}} k_z, \end{aligned} \tag{2}$$

where ν_{21} is the 21-cm frequency in the rest frame of emitting atoms, $H(z)$ iz the Hubble parameter, $\chi(z)$ is the comoving distance to redshift z, which marks the middle of the observed data cube (where r_z and θ_ν intervals are evaluated). Note that conditions of the type $2\pi\theta_x u = r_x k_x$ are saticefied.

The convention we use for the Fourier transforms is (note that Fourier-space functions are denoted with tilde)

$$\begin{aligned} I(\vec{r}) &= \frac{1}{(2\pi)^3} \int \widetilde{I}(\vec{k}) e^{i\vec{k}\cdot\vec{r}} d\vec{k}, \\ \widetilde{I}(\vec{k}) &= \int I(\vec{r}) e^{-i\vec{k}\cdot\vec{r}} d\vec{r}, \end{aligned} \tag{3}$$

and similarly,

$$\begin{aligned} \mathcal{I}(\theta_x, \theta_y, \theta_\nu) &= \int \widetilde{\mathcal{I}}(u, v, \eta) e^{2\pi i (u\theta_x + v\theta_y + \eta\theta_\nu)} du dv d\eta, \\ \widetilde{\mathcal{I}}(u, v, \eta) &= \int \mathcal{I}(\theta_x, \theta_y, \theta_\nu) e^{-2\pi i (u\theta_x + v\theta_y + \eta\theta_\nu)} d\theta_x d\theta_y d\theta_\nu. \end{aligned} \tag{4}$$

The following scaling relation is saticefied

$$\widetilde{I}(\vec{k}) = \frac{c(1+z)^2 \chi(z)^2}{H(z)\nu_{21}} \widetilde{\mathcal{I}}(u, v, \eta), \tag{5}$$

where the proportionallity factor contains a Jacobian $\frac{dr_x dr_y dr_z}{d\theta_x d\theta_y d\theta_\nu}$. Finally, the relationship between the specific intensity in the uv-plane and the visibility function $V(u, v, \theta_\nu)$ is given by a Fourier transform over only the frequency coordinate,

$$\begin{aligned} V(u, v, \theta_\nu) &= \int \widetilde{\mathcal{I}}(u, v, \eta) e^{2\pi i \theta_\nu \eta} d\eta, \\ \widetilde{\mathcal{I}}(u, v, \eta) &= \int V(u, v, \theta_\nu) e^{-2\pi i \theta_\nu \eta} d\theta_\nu, \end{aligned} \tag{6}$$

Here, $\theta_{\nu,\max} - \theta_{\nu,\min} = \Delta\nu$ is the bandwidth of the observed data cube centered on z (see also Appendix A).

B. Power spectra and noise

In this Section, we derive the noise power spectrum for the brightness temperature signal. We start by defining a brightness-temperature power spectrum as

$$\langle \widetilde{I}(\vec{k}) \widetilde{I}^*(\vec{k}') \rangle \equiv (2\pi)^3 P_{\widetilde{I}} \delta_D(\vec{k} - \vec{k}'), \tag{7}$$

where δ_D is the Dirac delta function. The observable we wish to relate this power spectrum to is the visibility function—a complex Gaussian variable with a zero mean, whose noise-induced variance (derived in Appendix A) reads

$$\begin{aligned} &\langle V(u, v, \theta_\nu) V(u', v', \theta'_\nu)^* \rangle \\ &= \frac{1}{\Omega_{\rm beam}} \left(\frac{2k_B T_{\rm sky}}{A_e \sqrt{\Delta\nu t_1}} \right)^2 \delta_D(u - u') \delta_D(v - v') \delta_{\theta_\nu \theta'_\nu}, \end{aligned} \tag{8}$$

where $T_{\rm sky}$ is the sky temperature; t_1 is the total time a single baseline spent observing an element at the position (u, v) in the uv plane; A_e is the collecting area of a single

dish; k_B is Boltzmann constant; $\Delta\nu$ is the bandwidth centered on z; and δ symbol with subscripts denotes the Kronecker delta.

The next step is to combine Eqs. (6) and (8), and take ensamble average to get

$$\langle\widetilde{\mathcal{I}}(u,v,\eta)\widetilde{\mathcal{I}}^*(u',v',\eta')\rangle = \frac{1}{t_1\Omega_{\rm beam}}\left(\frac{2k_BT_{\rm sky}}{A_e}\right)^2\delta_D(u-u')\delta_D(v-v')\delta_D(\eta-\eta'), \quad (9)$$

where

$$\int e^{2\pi i\theta_\nu(\eta-\eta')}d\theta_\nu = \delta_D(\eta-\eta'), \quad (10)$$

is the periodic delta-function on the t_1 interval. Taking into account the scaling relation of Eq. (5), introducing the power spectrum of Eq. (7), and keeping in mind the scaling property of the delta function, we arrive at

$$P_1^N(\vec{k}) = \frac{c(1+z)^2\chi^2(z)}{\Omega_{\rm beam}t_1H(z)\nu_{21}}\left(\frac{2k_BT_{\rm sky}}{A_e}\right)^2, \quad (11)$$

for the noise per $\vec{k}$ mode, per baseline.

Computation of t_1 from the total duration of the survey $t_{\rm obs}$ depends on the type of the experiment. For a beam of a solid angle $\Omega_{\rm beam} = \lambda^2/A_e$ much smaller than the solid angle of the entire survey, $\Omega_{\rm survey}$, where telescopes scan the sky one beamwidth at a time (such as the case for radio dishes), t_1 is the total time spent observing one uv element of size corresponding to the beam size, $t_1 = t_{\rm obs}\Omega_{\rm survey}/\Omega_{\rm beam}$. However, in the case of an array of dipoles, the beam is greater or equal to the survey angular size, and $t_1 = t_{\rm obs}$. When deriving numerical results in §VI, we will assume the latter. Finally, we will not account for the fact that a given patch of the sky is only visible for a part of a day from a given location; therefore, $t_{\rm obs}$ we use in §VI is the survey duration times a factor of a few or less that corrects for this assumption.

The last step is to get from Eq. (11) to the expression for the noise power spectrum that corresponds to the observation with all the available baselines. To do that, we need to incorporate the knowledge about the array configuration and the coverage of the uv plane. In other words, we need to divide the expression in Eq. (11) by the number of baselines that see a given mode $\vec{k}$ at any given time $n_{\rm base}(\vec{k})$ (for a discussion of the uv coverage, see the following section). The final result for the noise power spectrum per mode $\vec{k}$ in the intensity units is then

$$P^N(\vec{k}) = \frac{c(1+z)^2\chi^2(z)}{\Omega_{\rm beam}t_1H(z)\nu_{21}}\frac{(2k_BT_{\rm sky})^2}{A_e^2n_{\rm base}(\vec{k})}, \quad (12)$$

and in temperature units

$$P^N(\vec{k}) = \frac{\lambda^4c(1+z)^2\chi^2(z)}{\Omega_{\rm beam}t_1H(z)\nu_{21}}\frac{T_{\rm sky}^2}{A_e^2n_{\rm base}(\vec{k})}. \quad (13)$$

C. The UV coverage

Total number density $n_{\rm base}(\vec{k})$ of baselines that can observe mode $\vec{k}$ is related to the (unitless) number density $n(u,v)$ of baselines per $dudv$ element as

$$n_{\rm base}(\vec{k}) = \frac{n(u,v)}{\Omega_{\rm beam}}, \quad (14)$$

where $\frac{1}{\Omega_{\rm beam}}$ represents an element in the uv plane. The number density integrates to the total number of baselines $N_{\rm base}$,

$$N_{\rm base} = \frac{1}{2}N_{\rm ant}(N_{\rm ant}+1) = \int_{\rm half}n(u,v)dudv, \quad (15)$$

where $N_{\rm ant}$ is the number of antennas in the array, and the integration is done on the half of the uv plane (because the visibility has the following property $V(u,v,\theta_\nu) = V^*(-u,-v,\theta_\nu)$, and only half the plane contains independent samples). We assume that the array consists of many antennas, so that time-dependence of $n(u,v)$ is negligible; if this is not the case, one should compute its time average to account for Earth's rotation.

Let us now consider $n_{\rm base}(\vec{k})$ for a specific array configuration that is of particualr interest to cosmology—a tightly packed array of simple dipole antennas, tiling a squared-surface of the area $(\Delta L)^2$ with a filling fraction close to one. This is a design such as the Fast Fourier Transform Telescope (FFTT) described in [**?**]. In this case, the beam solid angle is 1 sr, the affective area of a single dipole is $A_e = \lambda^2$, and the effective number of antennas is then $N_{\rm ant} = \frac{(\Delta L)^2}{\lambda^2}$. For such configuration

$$n(u,v) = (\frac{\Delta L}{\lambda}-u)(\frac{\Delta L}{\lambda}-v). \quad (16)$$

The relation between $\vec{k} = (k,\theta_k,\phi_k)$ and (u,v) is

$$\begin{aligned} u_\perp &\equiv \frac{\chi(z)}{2\pi}k\sin\theta_k, \\ u &= u_\perp\cos\phi_k, \\ v &= u_\perp\sin\phi_k, \end{aligned} \quad (17)$$

where subscript $\perp$ denotes components perpendicular to the LOS direction $\widehat{\mathbf{n}}$. From this, the corresponsing number of baselines observing a given $\vec{k}$ is

$$\begin{aligned} n_{\rm base}(\vec{k}) = (&\frac{\Delta L}{\lambda}-\frac{\chi(z)}{2\pi}k\sin\theta_k\cos\phi_k) \\ \times(&\frac{\Delta L}{\lambda}-\frac{\chi(z)}{2\pi}k\sin\theta_k\sin\phi_k). \end{aligned} \quad (18)$$

In §VI, we use a ϕ_k-averaged version of this quantity (between 0 and $\pi/2$ only, due to the four-fold symmetry of the experimental setup of a square of dipoles), to account for the rotation of the baselines with respect to the

modes,

$$\langle n_{\rm base}(\vec{k})\rangle_{\phi_k} = \left(\frac{\Delta L}{\lambda}\right)^2 - \frac{4}{\pi}\frac{\Delta L}{\lambda}\frac{\chi(z)}{2\pi}k\sin\theta_k + \left(\frac{\chi(z)}{2\pi}k\sin\theta_k\right)^2. \quad (19)$$

IV. QUADRATIC ESTIMATOR FORMALISM

We now derive an unbiased minimum-variance quadratic estimator for a cosmic magnetic field $\vec{B}$, following a formalism similar to what is used in CMB studies [**?**]. In the following, we assume that the field only evolves with redshift due to the expansion of the universe (adiabatically) as

$$B(z) = B_0(1+z)^2, \quad (20)$$

where B_0 represents its present-day value (or equivalently, its value in comoving units), where the relevant estimator is denoted with a hat sign, $\widehat{B}_0$. We first consider the case of a field uniform in the entire survey volume, described by a single parameter, B_0. Then we move on to the case of a stochastic magnetic field, with a given power spectrum $P_B(\vec{K})$ where $\vec{K}$ denotes the wavevector for the mode of the field; in this case, the relevant estimator is of its amplitude, $\widehat{A}_0^2$. In both cases, the presented formalism is only valid if there the following separation is scales is saticefied: density-field modes in consideration must have much smaller wavelengths than the coherence scale of the magnetic field (or a given mode of a stochastic magnetic field), and both must be smaller than the size of the tomography survey at hand.

A. Uniform field

We first derive an unbiased minimum-variance quadratic estimator $\widehat{B}_0$ for a comoving uniform magnetic field. We start by noting that the redshifted 21-cm brightness temperature Fourier modes $T(\vec{k})$ contain contribution from the noise $T^N(\vec{k})$ and the signal $T^S(\vec{k})$, where the signal is contains contributions from the 21-cm signal with no magnetic field (null-case signal $T_0^S(\vec{k})$), and with the magnetic field,

$$T(\vec{k}) = T^N(\vec{k}) + T^S(\vec{k}),$$
$$T^S(\vec{k}) = T_0^S(\vec{k}) + B_0\frac{\partial T_0^S}{\partial B_0}(\vec{k}), \quad (21)$$

where B is a small expansion parameter (we adopt the linear-theory approach throught this work). We use the subscript "0" to denote functions evaluated at $B = 0$. Temperature is proportional to is the density fluctuation δ, with the transfer funtion $G(\widehat{\mathbf{k}})$ as the proportionality factor, such that

$$G \equiv \frac{dT}{d\delta}(\delta = 0), \quad (22)$$

and

$$T^S(\vec{k}) = G(\widehat{\mathbf{k}})\delta(k),$$
$$T_0^S(\vec{k}) = G_0(\widehat{\mathbf{k}})\delta(k), \quad (23)$$

where $\widehat{\mathbf{k}} = (\theta_k, \phi_k)$ is a unit vector in the direction of $\vec{k}$. Note that while G is a function of the direction vector $\widehat{\mathbf{k}}$ only, the power spectrum P_δ is a function of the magnitude k, in an isotropic universe. For simplicity of the expressions, we adopt the following notation

$$\frac{\partial T_0^S}{\partial B_0}(\vec{k}) \equiv \delta(k)\frac{\partial G}{\partial B_0}(\widehat{\mathbf{k}}, B_0 = 0),$$
$$\frac{\partial G_0}{\partial B_0}(\widehat{\mathbf{k}}) \equiv \frac{\partial G}{\partial B_0}(\widehat{\mathbf{k}}, B_0 = 0). \quad (24)$$

Since in the rest of this work we assume adiabatic evolution of the magnetic field, it is worth noting that $\frac{\partial G_0}{\partial B_0} = \frac{\partial G_0}{\partial B}(1+z)^2$. Furthermore, we denote the power spectrum in the null case as

$$P_{\rm null}(\vec{k}) \equiv P^N(\vec{k}) + P_0^S(\vec{k}). \quad (25)$$

The signal power spectrum in the absence of a magnetic fields is given as

$$\left\langle T_0(\vec{k})T_0^*(\vec{k}')\right\rangle \equiv (2\pi)^3\delta_D(\vec{k}-\vec{k}')P_0^S(\vec{k}) = (2\pi)^3\delta_D(\vec{k}-\vec{k}')G_0^2(\widehat{\mathbf{k}})P_\delta(k), \quad (26)$$

where

$$\left\langle \delta(\vec{k})\delta^*(\vec{k}')\right\rangle \equiv (2\pi)^3\delta_D(\vec{k}-\vec{k}')P_\delta(k). \quad (27)$$

The observable 2-point correlation function in Fourier space is

$$\langle T(\vec{k})T^*(\vec{k}')\rangle = P_{\rm null}(\vec{k})(2\pi)^3\delta_D(\vec{k}-\vec{k}') + \langle T_0^S(\vec{k})B_0\frac{\partial T_0^{S,*}}{\partial B_0}(\vec{k}')\rangle + \langle T_0^{S,*}(\vec{k}')B_0\frac{\partial T_0^S}{\partial B_0}(\vec{k})\rangle = \left(P_{\rm null}(\vec{k}) + 2B_0P_\delta(k)G_0(\widehat{\mathbf{k}})\frac{\partial G}{\partial B_0}(\widehat{\mathbf{k}})\right) \times(2\pi)^3\delta_D(\vec{k}-\vec{k}'), \quad (28)$$

where we assume that the signal and the noise are uncorrelated and keep only terms linear in B_0, and used the reality of G_0 and $\frac{\partial G}{\partial B_0}$.

Since we observe only one universe, the measured proxy for the ensamble average in Eq. (28) is the product $T(\vec{k})T^*(\vec{k})$. Using Eq. (28), each $T(\vec{k})$ gives an estimate for B_0,

$$\widehat{B}_0^{\vec{k}} = \frac{\frac{1}{V}T(\vec{k})T^*(\vec{k}) - P_{\rm null}(\vec{k})}{2P_\delta(k)G_0(\widehat{\mathbf{k}})\frac{\partial G_0}{\partial B_0}(\widehat{\mathbf{k}})}, \quad (29)$$

where we use the following property of the Dirac delta function on a finite volume of the survey V

$$\delta_D(\vec{k}-\vec{k}') = \frac{V}{(2\pi)^3}, \qquad \text{for } \vec{k}=\vec{k}', \tag{30}$$

related to the Kroneker delta,

$$\delta_{\vec{k}\vec{k}'} = \frac{(2\pi)^3}{V}\delta_D(\vec{k}-\vec{k}'), \tag{31}$$

and the following normalization convention

$$(2\pi)^3\delta_D(\vec{k}-\vec{k}') \equiv \int d\vec{r}e^{-i\vec{r}\cdot(\vec{k}-\vec{k}')}. \tag{32}$$

The estimator of Eq. (29) is unbiased, $\langle\widehat{B}_0^{\vec{k}}\rangle = 0$. The covariance of the estimates from all available temperature-field modes $\langle\widehat{B}_0^{\vec{k}}\widehat{B}_0^{\vec{k}',*}\rangle$ involves temperature-field 4-point correlation with three Wick constractions; its numerator reads

$$\begin{aligned}
&\frac{1}{V^2}\langle T(\vec{k})T^*(\vec{k})T(\vec{k}')T^*(\vec{k}')\rangle + P_{\rm null}(\vec{k})P_{\rm null}(\vec{k}') \\
&-\frac{1}{V}P_{\rm null}(\vec{k})\langle T(\vec{k}')T^*(\vec{k}')\rangle - \frac{1}{V}P_{\rm null}(\vec{k}')\langle T(\vec{k})T^*(\vec{k})\rangle \\
&= P_{\rm null}(\vec{k})P_{\rm null}(\vec{k}')\left[\frac{(2\pi)^6}{V^2}\,\delta_D(\vec{k}-\vec{k})\delta_D(\vec{k}'-\vec{k}')\right. \\
&+\frac{(2\pi)^6}{V^2}\delta_D(\vec{k}-\vec{k}')\delta_D(\vec{k}-\vec{k}') + \frac{(2\pi)^6}{V^2}\delta_D(\vec{k}+\vec{k}')\delta_D(\vec{k}+\vec{k}') \\
&\left.-\frac{(2\pi)^3}{V}\delta_D(\vec{k}'-\vec{k}') - \frac{(2\pi)^3}{V}\delta_D(\vec{k}-\vec{k})\right] \\
&= P_{\rm null}(\vec{k})P_{\rm null}(\vec{k}')\left(\delta_{\vec{k},\vec{k}'} + \delta_{\vec{k},-\vec{k}'}\right)
\end{aligned} \tag{33}$$

where every ensamble average yielded one factor of V. Finally, we get the following expression

$$\langle\widehat{B}_0^{\vec{k}}\widehat{B}_0^{\vec{k}',*}\rangle = \frac{P_{\rm null}^2(\vec{k})\left(\delta_{\vec{k},\vec{k}'} + \delta_{\vec{k},-\vec{k}'}\right)}{4P_\delta(k)^2\left[G_0(\widehat{\mathbf{k}})\frac{\partial G_0}{\partial B_0}(\widehat{\mathbf{k}})\right]^2}, \tag{34}$$

Estimates coming from different $\vec{k}$-modes can be combined with inverse-variance weights in the usual way to form a minimum-variance estimator,

$$\widehat{B}_0 = \frac{\sum_{\vec{k}}\frac{\widehat{B}_0^{\vec{k}}}{\langle\widehat{B}_0^{\vec{k}}\widehat{B}_0^{\vec{k},*}\rangle}}{\sum_{\vec{k}}\frac{1}{\langle\widehat{B}_0^{\vec{k}}\widehat{B}_0^{\vec{k},*}\rangle}}. \tag{35}$$

The final expression for the minimum-variance quadratic estimator computed from temperature measurements at a given redshift is

$$\begin{aligned}
\widehat{B}_0 = \sigma^2_{\widehat{B}_0}\sum_{\vec{k}}&\frac{\frac{1}{V}T(\vec{k})T^*(\vec{k}) - P_{\rm null}(\vec{k})}{P_{\rm null}^2(\vec{k})} \\
&\times 2P_\delta(k)G_0(\widehat{\mathbf{k}})\frac{\partial G_0}{\partial B_0}(\widehat{\mathbf{k}}),
\end{aligned} \tag{36}$$

with variance given by

$$\sigma^{-2}_{\widehat{B}_0} = \frac{1}{2}\sum_{\vec{k}}\left(\frac{2P_\delta(k)G_0(\widehat{\mathbf{k}})\frac{\partial G_0}{\partial B_0}(\widehat{\mathbf{k}})}{P_{\rm null}(\vec{k})}\right)^2, \tag{37}$$

where the sums are over the whole $\vec{k}$-plane.[1]

B. Stochastic field

We now derive a minimum-variance quadratic estimator for Fourier modes of a stochastic magnetic field. Note that in this Section we do *not* assume a particular model for its power spectrum. We use B_0 to denote a component of the magnetic field along one of the three Cartesian-system axes, and $\vec{r}$ to denote a position vector in physical space. We start with

$$T(\vec{r}) = T_0(\vec{r}) + B_0(\vec{r})\frac{\partial T_0^S}{\partial B_0}(\vec{r}), \tag{38}$$

where the subscripts and superscripts have the same meaning as before. Note that the distinction from the uniform field case is that the components of the magnetic field are now functions of $\vec{r}$. In Fourier space, we have

$$\begin{aligned}
T(\vec{k}) &= T_0(\vec{k}) + \int d\vec{r}e^{-i\vec{k}\cdot\vec{r}}B_0(\vec{r})\frac{\partial T_0^S}{\partial B_0}(\vec{r}) \\
&= T_0(\vec{k}) + \frac{1}{(2\pi)^3}\int d\vec{k}_1 B_0(\vec{k}_1)\frac{\partial T_0^S}{\partial B_0}(\vec{k}-\vec{k}_1),
\end{aligned} \tag{39}$$

where the last step used the convolution theorem.

In this case, the observable 2-point correlation function in Fourier space becomes

$$\begin{aligned}
\left\langle T(\vec{k})T^*(\vec{k}')\right\rangle &= (2\pi)^3\delta_D(\vec{k}-\vec{k}')P_{\rm null}(\vec{k}) \\
&+\left\langle T_0^{S,*}(\vec{k}')\frac{1}{(2\pi)^3}\int d\vec{k}_1 B_0(\vec{k}_1)\frac{\partial T_0^S}{\partial B_0}(\vec{k}-\vec{k}_1)\right\rangle \\
&+\left\langle T_0^S(\vec{k})\frac{1}{(2\pi)^3}\int d\vec{k}_1 B_0^*(\vec{k}_1)\left(\frac{\partial T_0^S}{\partial B_0}(\vec{k}'-\vec{k}_1)\right)^*\right\rangle,
\end{aligned} \tag{40}$$

to first order in B_0. Using Eqs. (23), (24), and (27), we further get

$$\begin{aligned}
\left\langle T(\vec{k})T^*(\vec{k}')\right\rangle &= (2\pi)^3\delta_D(\vec{k}-\vec{k}')P_{\rm null}(\vec{k}) + B_0(\vec{k}-\vec{k}') \\
&\times\left[P_\delta(k')G_0^*(\widehat{\mathbf{k}}')\frac{\partial G_0}{\partial B_0}(\widehat{\mathbf{k}}') + P_\delta(k)G_0(\widehat{\mathbf{k}})\frac{\partial G_0^*}{\partial B_0}(\widehat{\mathbf{k}})\right],
\end{aligned} \tag{41}$$

[1] Note that $\widehat{B}_0^{\vec{k}} = \widehat{B}_0^{-\vec{k}}$, following from the reality condition on the temperature field, $T(\vec{k}) = T^*(-\vec{k})$, and the isotropy of space in the null-assumption case, $G(\widehat{\mathbf{k}}) = G(-\widehat{\mathbf{k}})$, which is why the factor of 1/2 appears in order to avoid double-counting of modes.

where we also used the reality of the B_0 field that warrants $B_0^*(-\vec{K}) = B_0(\vec{K})$. Now, using a procedure analogous to that presented in §IV A, we can estimate $B_0(\vec{K} \equiv \vec{k} - \vec{k}')$ from $\vec{k}\vec{k}'$ pair of mode measurements in the temperature field as

$$\widehat{B}_0^{\vec{k}\vec{k}'}(\vec{K}) = \frac{T(\vec{k})T^*(\vec{k}')}{P_\delta(k')G_0^*(\widehat{\mathbf{k}}')\frac{\partial G_0}{\partial B_0}(\widehat{\mathbf{k}}') + P_\delta(k)G_0(\widehat{\mathbf{k}})\frac{\partial G_0^*}{\partial B_0}(\widehat{\mathbf{k}})}, \tag{42}$$

where we only focus on terms $\vec{K} \neq 0$ ($\vec{k} \neq \vec{k}'$). The variance $\left\langle \widehat{B}_0^{\vec{k}\vec{k}'}(\vec{K}) \left(\widehat{B}_0^{\vec{k}\vec{k}'}(\vec{K}')\right)^* \right\rangle$ of this estimator under the null assumption can we evaluated trivially from the above expression. Finally, from Eq. (42), we can derive the full estimator for the mode $B_0(\vec{K})$, in the usual way—by combining the individual $\widehat{B}_0^{\vec{k}\vec{k}'}(\vec{K})$ estimates with inverse-variance weights, and normalizing appropriately. However, for the purpose of detectability analysis, we are only interested in the variance of that estimator, or equivalently, the noise power spectrum of $\widehat{B}_0$, given by

$$(2\pi)^3\delta_D(\vec{K} - \vec{K}')P_{B_0}^N(\vec{K}) \equiv \left\langle \widehat{B}_0(\vec{K})\widehat{B}_0(\vec{K}')^* \right\rangle$$
$$= \left(\sum_{\vec{k}} \frac{\left(P_\delta(k')G_0^*(\widehat{\mathbf{k}}')\frac{\partial G_0}{\partial B_0}(\widehat{\mathbf{k}}') + P_\delta(k)G_0(\widehat{\mathbf{k}})\frac{\partial G_0^*}{\partial B_0}(\widehat{\mathbf{k}})\right)^2}{2V^2 P_{\rm null}(\vec{k})P_{\rm null}(\vec{k}')} \right)^{-1} \tag{43}$$

with the restriction $\vec{K} = \vec{k} - \vec{k}'$. Factor of 2 in the denominator corrects for double-counting mode pairs since $\widehat{B}_0^{\vec{k}\vec{k}'}(\vec{K}) = \left(\widehat{B}_0^{-\vec{k}-\vec{k}'}(\vec{K})\right)^*$, and the sum in the above expression is unconstrained. If we only consider diagonal terms $\vec{K} = \vec{K}'$, then the LHS of the above expression becomes equal to $VP_{B_0}^N(\vec{K})$. The explicit expression for the noise power spectrum is then

$$P_{B_0}^N(\vec{K}) =$$
$$\left(\sum_{\vec{k}} \frac{\left(P_\delta(k')G_0^*(\widehat{\mathbf{k}}')\frac{\partial G_0}{\partial B_0}(\widehat{\mathbf{k}}') + P_\delta(k)G_0(\widehat{\mathbf{k}})\frac{\partial G_0^*}{\partial B_0}(\widehat{\mathbf{k}})\right)^2}{2V P_{\rm null}(\vec{k})P_{\rm null}(\vec{k}')} \right)^{-1}, \tag{44}$$

Note that only the components of the magnetic field in the plane of the sky have an effect of the observed brightness temperature, and so the above expression represents the noise power spectrum for either one of those two (uncorrelated) components. The noise in the direction along the line of sight can be considered infinite. Finally, note that a similar type of estimator can be written down for the direction of the magnetic field in a given patch of the sky. However, in this work we only focus on the magnitude of the field.

V. FISHER ANALYSIS

We now use the key results of §IV to evaluate expressions for sensitivity of future observations. We first derive the expression for sensitivity to a field uniform in the entire survey volume. We start with the unsatured case, and consider the limit where the field (in the classical picture) produces less than 1 radian of precession at all redshifts of interest, and then move on to the saturated (strong field) limit. Secondly, we derive the expression for sensitivity to detecting a stochastic magnetic field with a scale-independent power spectrum.

A. Uniform field case

For a measurement of the redshifted 21-cm brightness temperature signal at a given z, the sensitivity $\sigma_{\widehat{B}_0}$ to recovering a uniform field B_0 in unsaturated limit is given by Eq. (37). The total sensitivity of a tomorgraphy survey over a range of redshifts is given by

$$\sigma_{B_0}^{-2} = \frac{1}{2}\int dV(z)\frac{k^2 dk d\phi_k \sin\theta_k d\theta_k}{(2\pi)^3}$$
$$\times \left(\frac{2P_\delta(k,z)G_0(\theta_k,\phi_k,z)\frac{\partial G_0}{\partial B_0}(\theta_k,\phi_k,z)}{P^N(k,\theta_k,z) + P_\delta(k,z)G_0^2(\theta_k,\phi_k,z)} \right)^2, \tag{45}$$

where we transitioned from a sum over $\vec{k}$ modes to an integral, using $\sum_{\vec{k}} \to V\int d\vec{k}/(2\pi)^3$. The integral is performed over the (comoving) volume of the survey of angular size $\Omega_{\rm survey}$ (in steradians) at a given redshift,

$$dV = \frac{c}{H(z)}\chi^2(z)\Omega_{\rm survey}dz, \tag{46}$$

and the integration limits are: $\phi_k \in [0, 2\pi]$; $\theta_k \in [0, \pi]$; and $k \in [2\pi u_{\rm min}/(d_A \sin\theta_k), 2\pi u_{\rm max}/(d_A \sin\theta_k)]$, where $u_{\rm min,max} = \frac{L_{\rm min,\ max}}{\lambda}$ correspond to the maximum and minimum baseline $L_{\rm min}$ and $L_{\rm max}$, respectively. If the survey area is big enough that the flat-sky approximation breaks down, $\sigma_{B_0}^{-2}$ can be computed on small (approximately flat) patch $\Omega_{\rm patch}$, and corrected in the following way to account for the total survey volume [2]

$$\sigma_{\widehat{B}_0,\ {\rm tot}}^{-2} = \frac{\sigma_{\widehat{B}_0}^{-2}}{\Omega_{\rm patch}}\int_0^{\theta_{\rm survey}}\int_0^{2\pi}\cos^2\theta d\theta d\phi$$
$$= \frac{\sigma_{\widehat{B}_0}^{-2}\pi}{\Omega_{\rm patch}}\left(\theta_{\rm survey} + \cos\theta_{\rm survey}\sin\theta_{\rm survey}\right). \tag{47}$$

Let us now consider a field that is strong enough to produce precession by more than a radian in a lifetime

[2] This accounts for the change in the angle that a uniform magnetic field makes with a line of sight, as the line of sight moves through a large survey area.

of the excited state of the 21-cm transition; this is the saturated-signal case. The brightness-temperature 2-point correlation functions still capture the presence of the field in this case (as illustrated in Figure 2), but it loses sensitivity to recovering its exact magnitude. Ability to distinguish staturated case from zero magnetic field becomes a relevant measure of sensitivity in this case.

To evaluate the sensitivity, we can write the signal power spectrum as a sum of contributions from $B_0 = 0$ and $B_0 \to \infty$ cases,

$$P^S(\vec{k}) = (1-\xi)P^S(\vec{k}, B=0) + \xi P^S(\vec{k}, B\to\infty), \quad (48)$$

and perform the standard Fisher analysis to evaluate sensitivity to recovering parameter ξ,

$$\sigma_\xi^{-2} = \int dV(z)\frac{d\vec{k}}{(2\pi)^3}\left(\frac{\frac{\partial P^S}{\partial\xi}(\vec{k})}{P^N(\vec{k}) + P_0^S(\vec{k}, \xi=0)}\right)^2. \quad (49)$$

In this case, we interpret σ_ξ as a 1σ sensitivity to *detecting* presence of a strong magnetic field.

B. Stochastic field case

Using Eq. (44) and a procedure analogous to the case of a uniform field, we get the following integral expression for the noise power spectrum of a plane-of-the-sky component of the magnetic field

$$\left(P^N_{B_{0,i}}(\vec{K})\right)^{-1} = \int k^2 dk \sin\theta_k d\theta_k d\phi_k \times \frac{\left(P_\delta(k')G_0^*(\widehat{\mathbf{k}}')\frac{\partial G_0}{\partial B_i}(\widehat{\mathbf{k}}') + P_\delta(k)G_0(\widehat{\mathbf{k}})\frac{\partial G_0^*}{\partial B_i}(\widehat{\mathbf{k}})\right)^2}{2(2\pi)^3 P_{\rm null}(\vec{k})P_{\rm null}(\vec{k}')}, \quad (50)$$

where $\vec{k}' = \vec{K} - \vec{k}$.

To compute signal-to-noise ratio (SNR) for measuring the amplitude of an arbitrary stochastic-field power spectrum in a given redshift slice z we need to perform a sum over all voxels (3d pixels) in the survey volume at that redshift. A general expression for SNR is

$$\mathrm{SNR}^2 = \frac{1}{2}Tr\left(N^{-1}SN^{-1}S\right), \quad (51)$$

where S and N are the signal and noise matrices. In our case, these are $3N_{\rm voxels}\times 3N_{\rm voxels}$ matrices (there are $N_{\rm voxels}$ voxels in the entire survey, and 3 components of the magnetic field). In the null case, voxels are independent, and so the noise matrix is diagonal, and the signal is captured by the 3d power spectrum of the magnetic field. The voxel-noise variance for measuring a single mode is given by $P^N_{B_{0,i}}(\vec{K}, z)/V_{\rm voxel}(z)$, where $V_{\rm voxel}$ is volume of a given voxel. Summing over voxels and components of the magnetic field with inverse-variance weights, for a single redshift slice, we get SNR as

$$\begin{aligned}\mathrm{SNR}^2(z) &= \frac{1}{2}\sum_{i\alpha,j\beta}\frac{S^2_{i\alpha,j\beta}}{P^N_{B_{0,i}}(\vec{K},z)P^N_{B_{0,j}}(\vec{K},z)}V^2_{\rm voxel} \\ &= \frac{1}{2}\sum_{ij}\int d\vec{r}_\alpha\int d\vec{r}_\beta\frac{\langle B_{0,i}(\vec{r}_\alpha)B_{0,j}(\vec{r}_\beta)\rangle^2}{P^N_{B_{0,i}}(\vec{K},z)P^N_{B_{0,j}}(\vec{K},z)},\end{aligned} \quad (52)$$

where we label voxels with Greek indicies, and, as before, retain Roman indicies for the field components; $\vec{r}_{\alpha/\beta}$ represents the spatial position of a given voxel.

To simplify further calculations, we now only focus on a particular class of magnetic-field models, where most of the power is on largest scales (small $\vec{K}$). In this (squeezed) limit, $\vec{K} \ll \vec{k}$ and thus $\vec{k} \approx \vec{k}'$, such that Eq. (50) reduces to the white noise (independent on $\vec{K}$). The model for the power spectrum is defined through

$$(2\pi)^3\delta_D(\vec{K}-\vec{K}')P_{B_{0,i}B_{0,j}}(\vec{K}) \equiv \left\langle B^*_{0,i}(\vec{K})B_{0,j}(\vec{K}')\right\rangle, \quad (53)$$

which relates to the variance in the transverse component $P_{B_\perp}(\vec{K})$ as

$$P_{B_{0,i}B_{0,j}}(\vec{K}) = (\delta_{ij} - \widehat{K}_i\widehat{K}_j)P_{B_\perp}(\vec{K}), \quad (54)$$

where $\widehat{K}_{i/j}$ is a unit vector along the direction of i/j component. In this discussion, as a concrete model example, we consider a scale–independent (SI) power spectrum,

$$P_{B_\perp}(\vec{K}) = A_0^2/K^3, \quad (55)$$

where the amplitude A_0 is a free parameter (in units of Gauss). Furthermore, if homogeneity and isotropy are satisfied, the integrand in Eq. (52) only depends on the separation vector $\vec{s} \equiv \vec{r}_\beta - \vec{r}_\alpha$. Using this and the squeezed limit assumption gives[3]

$$\begin{aligned}\mathrm{SNR}^2(z) &= \frac{1}{2}\sum_{ij}\frac{dV_{\rm patch}}{(P^N_{B_{0,i}}(z))^2}\int d\vec{s}\,\langle B_{0,}i(\vec{r}_\beta - \vec{s})B_{0,j}(\vec{r}_\beta)\rangle^2 \\ &= \frac{1}{2(2\pi)^3}\sum_{ij}\frac{dV_{\rm patch}}{(P^N_{B_{0,i}}(z))^2}\int d\vec{K}\left(P_{B_{0,i}B_{0,j}}(\vec{K})\right)^2,\end{aligned} \quad (56)$$

where $dV_{\rm patch}$ is the volume of a redshift–slice patch of Eq. (46). Substituting Eq. (55), and integrating over all z's available in the survey, total SNR reads

$$\mathrm{SNR}^2 = \frac{A_0^4}{2(2\pi)^3}\int_{z_{\rm min}}^{z_{\rm max}}\frac{dV_{\rm patch}}{(P^N_{B_{0,i}}(z))^2}\int_0^\pi\sin\theta d\theta \int_0^{2\pi}d\phi\int_{K_{\rm min}(z,\theta,\phi)}^{K_{\rm max}(z,\theta,\phi)}\frac{dK}{K^4}\sum_{ij\in\{xx,xy,yx,yy\}}(\delta_{ij}-\widehat{K}_i\widehat{K}_j)^2, \quad (57)$$

[3] Note that in the last step we used $\int d\vec{s}|f(\vec{s})|^2 = \int\frac{d\vec{K}}{(2\pi)^3}|\widetilde{f}(\vec{K})|^2$, which holds for an arbitrary function f and its Fourier transform $\widetilde{f}$.

where x and y denote components in the plane of the sky, and

$$\widehat{K}_x = \sin\theta\sin\phi,\ \ \widehat{K}_y = \sin\theta\cos\phi. \tag{58}$$

The sum in the above expression reduces to

$$\sum_{ij\in\{xx,xy,yx,yy\}} (\delta_{ij} - \widehat{K}_i\widehat{K}_j)^2 = 2\cos^2\theta + \sin^4\theta. \tag{59}$$

Substituting this into Eq. (57), and integrating over K, θ, ϕ gives

$$\mathrm{SNR}^2 = \frac{A_0^4}{10\pi^2}\int_{z_{\rm min}}^{z_{\rm max}} \frac{dV_{\rm patch}}{(P^N_{B_{0,i}}(z))^2}\left(\frac{1}{K^3_{\rm min}} - \frac{1}{K^3_{\rm max}}\right). \tag{60}$$

From this expression, 1σ sensitivity to measuring A_0^2 is

$$\sigma^2_{A_0^2} = \left[\frac{1}{10\pi^2}\int_{z_{\rm min}}^{z_{\rm max}} \frac{dV_{\rm patch}}{(P^N_{B_{0,i}}(z))^2}\left(\frac{1}{K^3_{\rm min}} - \frac{1}{K^3_{\rm max}}\right)\right]^{-1}. \tag{61}$$

VI. RESULTS

We now proceede to numerically evaluate the sensitivity of a tomographic 21-cm survey to detecting magnetic fields during the pre-reionization epoch, using the formalism of previous two Sections. For the purposes of deriving numerical results, we only focus on one type of experimental setup—an array of closely-packed dipole antennas, such as the FFTT considered in §III C. The motivation for this choice is the fact that such configuration is known to maximize sensitivity of measurements based on the 2-point statistics [**?**], such as the one we propose in this work. For the parameters of this survey, we assume that a surface area of $(\Delta L\ \mathrm{km})^2$ is covered in dipole antennas, and that the experiment observes $\Omega_{\rm survey} = 1\mathrm{sr}$ of the sky for about 5 years.[4] For the sky temperature that enters the calculation of the noise power spectrum in Eq. (13), we assume a simple model of Galactic foregrounds from [**?**], where

$$T_{\rm sky} = 60\left(\frac{21}{100}(1+z)\right)^{2.55}\ [\mathrm{K}]. \tag{62}$$

Furthermore, we assume that the redshift range covered by the survey is $z \in [15, 35]$. Other ingredients entering the sensitivity calculation are the Lyman-α flux $J_{\rm Ly\alpha}(z)$, and the spin and kinetic temperatures of the IGM; these

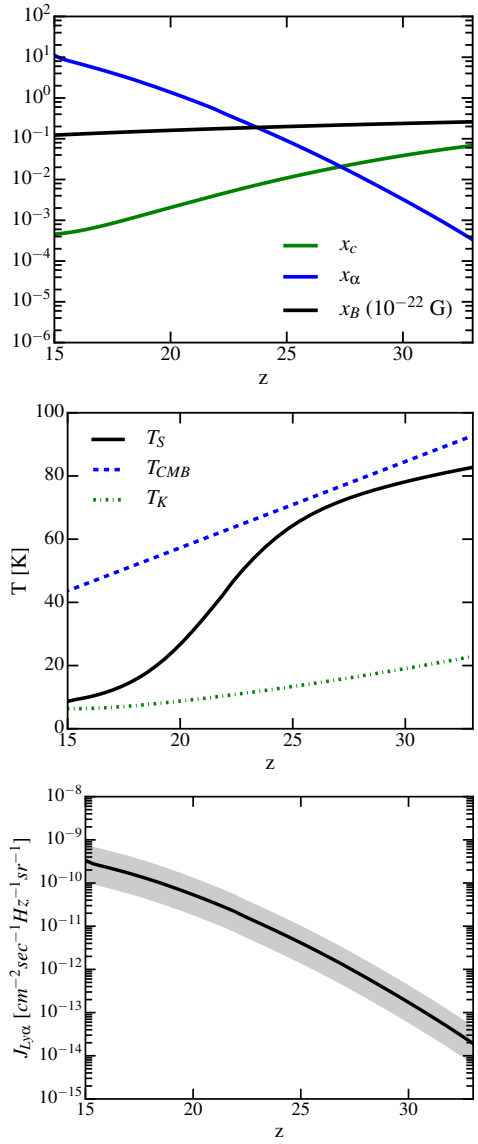

Figure 3. Inputs for sensitivity calculations: Lyman-α flux model, and the relevant spin- and kinetic- temperature models.

are obtained using `21CMFAST` [**?**], for standard cosmology, and are shown in Figure 3. We checked that the variation in the x-ray heating rate within a factor of a few from the fiducial model does not make significant changes to the presented results.

Figures 4 and 5 show how the sensitivity changes as a function of the maximum baseline ΔL (since different baselines may correspond to different stages of the experiment). Figure 4 shows 1σ sensitivity to measuring parameter ξ of Eq. (48), that distinguishes amongst the zero magnetic field case and the case where the field is strong enough that the signal saturates (in the sense described in §II). This parameter is by definition boud between the values of 0 and 1, where 0 represents the case of no magnetic field, and 1 represents the saturated

[4] The value used to evaluate Fisher formulas is actually 2 years. When corrected for the effect of Earth's rotation, and the fact that a given sky patch is above the horizon for only a fraction of a day, the effective observation time of 2 years translates to a (factor-of-a-few) longer wall-clock time.

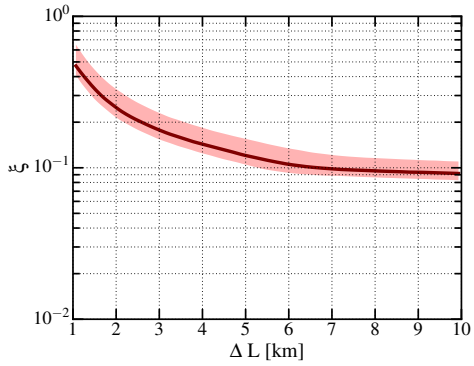

Figure 4. FFTT sensitivity to distinguishing saturated case from no magnetic field (upper panel), as a function of maximum array baseline, assuming a survey size of 1 sr, for survey duration of 2 years.

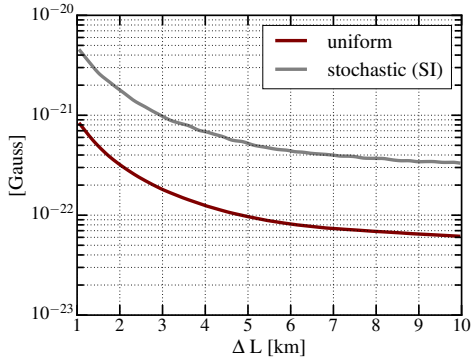

Figure 5. FFTT sensitivity to detecting a uniform and stochastic magnetic field (stochastic field is assumed to have a scale-independent (SI) power spectrum, and shown is the rms per $logK$, A_0/π.), as a function of maximum array baseline, assuming a survey size of 1 sr, for survey duration of 2 years.

case. From this Figure, we can see that, for example, a little over a square kilometer of covarega area is necessary for a 1σ detection of magnetic fields stronger than about 10^{-21} Gauss comoving. While this size of a radio array is still futuristic in terms of the shear number of antennas (compare to the SKA [**?**], for example), the number of mode measurements required for this measurement corresponds to the computational demands for the next-generation 21-cm cosmology experiment, and may thus be feasible in the coming couple of decades.

Figure 5 is obtained by evaluating the expressions of Eqs. (45) and (60), and shows sensitivity to measuring the scaled value of the magnetic field in the case of a uniform field (dark red line), and the sensitivity to measuring the amplitude of a particular model for a stochastic field (gray line)—the scale-independent (SI) power spectrum discussed in §V. While the numerical calculation behind this plot assumed that the brightness temperature is a linear function of the field strength, this assumption is not guaranteed to hold—it breaks in the saturation limit, as discussed in §II. In order to understand

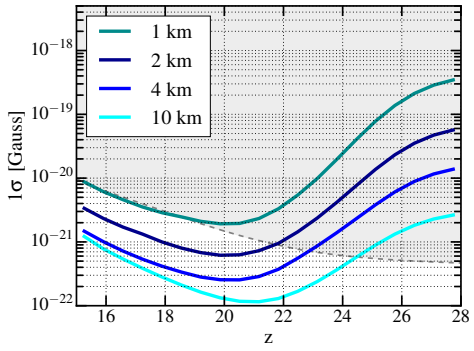

Figure 6. Saturation ceiling is shown as a shaded gray area, and integrand of Eq. (45) (inverse sqare root of it) is shown as a function of redshift, for several maximum baseline sizes. When the colored curves are below the saturation limit around their minima, the analysis assuming unsaturated regime is valid.

how the constraints (or, sensitivities) of Figure 5 compare to the saturation "ceiling" at the redshifts we integrate over, we present a rough calculation of the saturation as a function of redshift, and compare it to the values of the z-dependent integrands of Eq. (45). From this Figure, we can see that only above the coverage of about 16km^2 are we able to actually measure the exact value of the amplitude of the magnetic field power spectrum.

VII. CONCLUSIONS

In Paper I of this series, we proposed a new method to detect extremely weak magnetic fields in the IGM during the Dark Ages, using future 21-cm tomography experiments. In this paper, Paper II, we investigated sensitivity of future radio arrays using this method. We developed minimum-variance-estimator formalism that uses 2-point correlation function of the 21-cm brightness temperature to detect and measure magnetic fields in pre-reionization epoch.

Our results imply that the next-stage array with a little over a square kilometer of area covered in dipole antennas ina tightly-packed configuration, observing redshifts from 15 to 35, can in principle reach the sensitivity to detect magnetic fields on the order of 10^{-21} Gauss comoving. However, disentangling teh exact spectral shape of a stochastic field is more challenging, and can only be expected in the futuristic scenarios where arrays grow to a size of tens of square kilometers in coverage area. In this analysis, we took into account the noise arising from the presence of the large Galactic foreground signal, but we ignotered more subtle effects such as, for example, frequency dependence of the beams, etc., calculation of which would be necessary to create figures of merit for future experiements.

At the end, we emphasize again that the main limitation to sensitivity of this method to measuring magnetic

fields at high redshifts is a mere fact that it is based on a two-scattering process—as soon as quality of the 21-cm statistics reaches the levels necessary to probe second-order processes, the effect we focused on in this series of papers will immediately open up an "*in situ*" way to trace miniscule (and possibly primordial) magnetic fields with unprecedented precision.

ACKNOWLEDGMENTS

VG gratefully acknowledges the support from the W. M. Keck Foundation Fund. Illustrations in Figure 2 made use of HEALPix [**?**] software package[5].

Appendix A: Visibility-variance derivation

Here we derive the variance of the visibility for an interferometric array of two antennas separated by a baseline $\vec{b} = (b_x, b_y)$, each with an effective collecting area A_e, observing a single element in uv plane for time duration t_1, in the total bandwidth $\Delta\nu = \nu_{\rm max} - \nu_{\rm min}$. This setup is shown in Figure 7. Note that modes with frequencies that differ by less than $1/t_1$ cannot be distinguished in observation time t_1, and modes with frequencies in each interval of size $1/t_1$ are "collapsed" into a discrete mode with $\nu_n = n/t_1$, where $n \in Z$. Thus, the number of measured (discrete) frequencies is $N_\nu = t_1\Delta\nu$.

Electric field induced in a single antenna is

$$E(t) = \sum_n^{N_\nu} \widetilde{E}(\nu_n) e^{2\pi i \nu_n t}, \tag{A1}$$

while the quantity an interferometer measures is the correlation coefficient between the electric field in one, E_i, and the electric field in the other antenna, E_j, as a function of frequency,

$$\rho_{ij}(\nu) \equiv \frac{\langle \widetilde{E}_i^*(\nu)\widetilde{E}_j(\nu)\rangle}{\sqrt{\langle|\widetilde{E}_i(\nu)|^2\rangle\langle|\widetilde{E}_j(\nu)|^2\rangle}}. \tag{A2}$$

Let us now assume that

$$\langle \widetilde{E}_i^*(\nu_n)\widetilde{E}_j(\nu_m)\rangle = \sigma(\nu)^2\delta_{mn}, \tag{A3}$$

In the following, for clarity, we will omit writing the explicit dependence on ν. The real (or imaginary) part of ρ has the following variance

$$var(Re[\rho_{ij}])\frac{1}{2N_\nu} = \frac{1}{2t_1\Delta\nu}. \tag{A4}$$

Before continuing, let us take a brief digression to show that the above formula implicitly assumes that the electric fields in the two antennas $\widetilde{E}_i$ and $\widetilde{E}_j$ have a very weak correlation, $\rho \ll 1$. Namely, suppose x and y are random Gaussian variables with zero mean values, where $var(x) \equiv \langle (x - \langle x\rangle)^2\rangle = \langle x^2\rangle - \langle x\rangle^2 = \langle x^2\rangle$, and similarly for y, and their correlation coefficient is $\rho \equiv \frac{\langle xy\rangle}{\sqrt{\langle x^2\rangle\langle y^2\rangle}}$. In this case, the following is true

$$\begin{aligned} var(xy) &= \langle x^2y^2\rangle - \langle xy\rangle^2 = \langle x^2\rangle\langle y^2\rangle + \langle xy\rangle^2 \\ &= \langle x^2\rangle\langle y^2\rangle + \rho^2\langle x^2\rangle\langle y^2\rangle = var(x)var(y)(1+\rho^2), \end{aligned} \tag{A5}$$

so that when ρ is small $var(xy) = var(x)var(y)$, which was assumed in the first equality of Eq. (A4).

Resuming the derivation, if different frequencies are uncorrelated, the result of Eq. (A4) implies

$$\langle|\rho_{ij}(\nu)|^2\rangle = \frac{1}{t_1\Delta\nu}. \tag{A6}$$

The final step in this derivation requires the relation between intensity in the sky $\mathcal{I}(\theta_x, \theta_y, \nu)$ (within the beam of the solid angle $\Omega_{\rm beam}$, centered on the direction $\hat{\mathbf{n}} = (\theta_x, \theta_y)$) and the electric fields measured in the two antennas,

$$\begin{aligned} \langle \widetilde{E}_i^*(\nu)\widetilde{E}_j(\nu)\rangle \propto \int_{\Omega_{\rm beam}} d\theta_x d\theta_y \mathcal{I}(\theta_x, \theta_y, \theta_\nu) \\ \times e^{i\frac{2\pi\nu}{c}(b_x\theta_x + b_y\theta_y)} R(\theta_x, \theta_y), \end{aligned} \tag{A7}$$

where $R(\theta_x, \theta_y)$ is the antenna response function (the shape of the beam in the sky), which we will assume to be unity. Furthermore, $\frac{2\pi\nu}{c}(b_x\theta_x + b_y\theta_y) \equiv 2\pi(u\theta_x + v\theta_y)$ is the phase delay between two antennae (position in the uv plane measures the phase lag between the two dishes in wavelenghts). The coefficient of proportionallity in the above equation is set by various instrumental parameters, and is not relevant for our purposes. From Eq. (A2), it follows

$$\rho_{ij}(\nu) = \frac{\int_{\Omega_{\rm beam}} d\theta_x d\theta_y \mathcal{I}(\theta_x, \theta_y, \theta_\nu) e^{2\pi i(u\theta_x + v\theta_y)}}{\int_{\Omega_{\rm beam}} d\theta_x d\theta_y \mathcal{I}(\theta_x, \theta_y, \theta_\nu)}, \tag{A8}$$

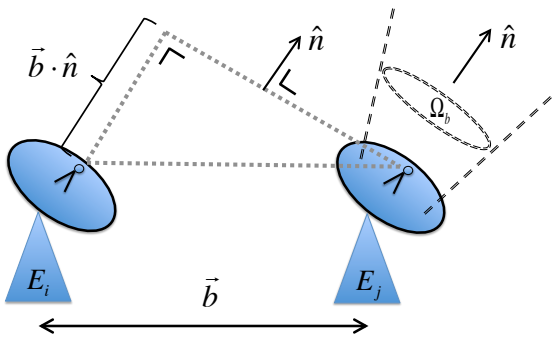

Figure 7. Schematic of a two-antenna interferometer.

[5] http://healpix.sf.net; https://github.com/healpy/healpy

where the denominator in the above formula approximately integrates to (for a small beam)

$$\int_{\Omega_{\rm beam}} d\theta_x d\theta_y \mathcal{I}(\theta_x,\theta_y,\theta_\nu) \approx \Omega_{\rm beam}\mathcal{I}(\theta_x,\theta_y,\theta_\nu). \quad \text{(A9)}$$

We can now use the approximate expression for the resolution of a single dish,

$$\Omega_{\rm beam} = \frac{\lambda^2}{A_e}, \quad \text{(A10)}$$

the Reyliegh-Jeans law (or the definition of the brightness temperature),

$$\mathcal{I}(\theta_x,\theta_y,\theta_\nu) = \frac{2k_B T_{\rm sky}}{\lambda^2}, \quad \text{(A11)}$$

and note that the numerator in Eq. (A8) matches the definition of visibility from Eq. (6) to get

$$\rho_{ij}(\nu) = \frac{A_e}{2k_B T_{\rm sky}} V(u,v,\theta_\nu), \quad \text{(A12)}$$

Combining the above expression and Eq. (A6), we get the final result of this derivation,

$$\langle |V(u,v,\theta_\nu)|^2\rangle = \frac{1}{\Omega_{\rm beam}}\left(\frac{2k_B T_{\rm sky}}{A_e\sqrt{t_1\Delta\nu}}\right)^2 \times\delta_D(u-u')\delta_D(v-v')\delta_{\theta_\nu\theta_{\nu'}}, \quad \text{(A13)}$$

where V is a complex Gaussian variable, centered at zero, and uncorrelated for different values of its arguments, and the factor of $\Omega_{\rm beam}$ came from converting from Kroneker to Dirac deltas.

It should be noted at the end that we were calculating the contribution to the visibility from the noise only (the system + the foregrounds in the absence of a signal), so we used system temperature for brightness temperature (this could contain the signal from foregrounds and from the instrument). In case we want to repeat the computation in the presence of a signal, $T_{\rm sky}$ should instead be the sum of the signal and the noise temperatures.

Appendix A: Lensing Magnetic Field Contamination

In this Appendix, we first briefly derive the power spectra of the transverse shear components of weak lensing. Then we estimate the magnetic field contamination due to lensing. At the end, we consider CMB lensing as an additional source of information to help diminish the contamination.

1. Transverse Shear Power Spectrum

The formalism for the two-dimensional weak lensing carried out, for example, in [**?**] is quite straightforward to be generalized to 3-dimensional case, where lensing maps the intrinsic image of sources on the sky, namely the source space, onto the observed sky, namely the image space. Any position on the sky can be denoted by its angular coordinates (θ_1,θ_2) and its comoving distance D or its redshift z.

Analogous to 2-dimensional weak lensing, we have

$$\theta_i^S = \theta_i + \frac{\partial\psi}{\partial\theta_i},\ i=1,2,3, \quad \text{(A1)}$$

representing that sources intrinsicly at position $(\theta_1^S,\theta_2^S,\theta_3^S)$ are related to the apparent position $(\theta_1,\theta_2,\theta_3)$ by the lensing potential ψ. Note that we assume the universe is flat, so that the angular coordinate components satisfy

$$\theta_i = \frac{\Delta x_i}{D},\ i=1,2,3, \quad \text{(A2)}$$

where $\Delta x_{1,2}$ is the comoving coordinates on the image plane near the source. The third coordinate Δx_3 is a small comoving deviation from the origin (which can be chosen arbitarily in the image space near the source) along the line of sight, so that it is related to redshift by $\Delta x_3 = \Delta z/H$.

By taking the derivative of Eqn.(A1), we find the Jacobian of the coordinate transformation from the image space to the source space,

$$\frac{\partial\theta_i^S}{\partial\theta_j} = \delta_{ij} + \frac{\partial^2\psi}{\partial\theta_i\partial\theta_j} = (1+\kappa)I_{ij} + \gamma_{ij}, \quad i,j=1,2,3, \quad \text{(A3)}$$

where we decompose the symmetric $\partial^2\psi/\partial\theta_i\partial\theta_j$ as the sum of a diagonal matrix and a symmetric traceless matrix $\boldsymbol{\gamma}$. They represent the effect of magnification and shear, respectively. There are 5 independent shear components.

Now we switch to the 2-dimentional Fourier space, i.e. from $\hat{n}\equiv(\theta_1,\theta_2)$ to $\vec{\ell}\equiv(\ell_1,\ell_2)$, where we put a tilde above the quantities. The $\tilde{\gamma}_{13},\tilde{\gamma}_{23}$ components are the transverse shear components that we care about. Let's calculate the power spectrum of γ_{13} first.

The 2D Fourier transform of the lensing potential is

$$\tilde{\psi}(\vec{\ell},D) = \int_\Omega \psi(D,\hat{n}) e^{-i\vec{\ell}\cdot\hat{n}}\, d\theta_1 d\theta_2. \quad \text{(A4)}$$

Note that the lensing potential ψ is given by

$$\psi(D,\hat{n}) = -2\int_0^D [\cot_K(D_1) - \cot_K(D)]\Phi(D_1,\hat{n}) dD_1, \quad \text{(A5)}$$

where Φ is the Newtonian gravitational potential and the cotangentlike function is hyperbolic for flat universe, i.e. $\cot_K(D) = 1/D$. One can show that

$$\frac{\partial\tilde{\psi}(\vec{\ell},z)}{\partial\theta_3} = -\frac{2}{D}\int_0^D dD_1 \tilde{\Phi}(D_1,\vec{\ell}), \quad \text{(A6)}$$

where $\tilde{\Phi}$ is the 2D Fourier transform of Φ. Now we obtain

$$\langle\tilde{\gamma}^*_{13}(\vec{\ell},z)\tilde{\gamma}_{13}(\vec{\ell}',z')\rangle = \left\langle \ell_1\ell_1' \frac{\tilde{\psi}^*(\vec{\ell},z)}{\partial\theta_3}\frac{\tilde{\psi}(\vec{\ell}',z')}{\partial\theta_3}\right\rangle$$
$$= \frac{4\ell_1\ell_1'}{D(z)D(z')}\int_0^{D(z)} dD_1 \int_0^{D(z')} dD_1' \langle\tilde{\Phi}^*(D_1,\vec{\ell})\tilde{\Phi}(D_1',\vec{\ell}')\rangle. \quad \text{(A7)}$$

Define

$$\tilde{\Phi}(D_1,\vec{\ell}) \equiv \int_{-\infty}^{\infty} \tilde{\tilde{\Phi}}(\ell_3,\vec{\ell}) e^{i\ell_3 D_1}\frac{d\ell_3}{2\pi}, \quad \text{(A8)}$$

we can write

$$\langle\tilde{\Phi}^*(D_1,\vec{\ell})\tilde{\Phi}(D_1',\vec{\ell}')\rangle = \int\int \frac{d\ell_3}{2\pi}\frac{d\ell_3'}{2\pi}\langle\tilde{\tilde{\Phi}}^*(\ell_3,\vec{\ell})\tilde{\tilde{\Phi}}(\ell_3',\vec{\ell}')\rangle \times e^{i(\ell_3' D_1' - \ell_3 D_1)}. \quad \text{(A9)}$$

Here $\tilde{\tilde{\Phi}}$ is actually the 3D Fourier transform of Φ, so we can assume that different modes are uncorrelated, which implies

$$\langle\tilde{\tilde{\Phi}}^*(\ell_3,\vec{\ell})\tilde{\tilde{\Phi}}(\ell_3',\vec{\ell}')\rangle = (2\pi)^3\delta(\ell_3-\ell_3')\delta^2(\vec{\ell}-\vec{\ell}')P_\Phi(\sqrt{\ell_3^2+|\vec{\ell}|^2}). \quad \text{(A10)}$$

Substituting into Eqn.(A9) and applying the Limber's approximation: $\ell_3 \ll |\vec{\ell}|$, we obtain

$$\langle\tilde{\Phi}^*(D_1,\vec{\ell})\tilde{\Phi}(D_1',\vec{\ell}')\rangle \simeq (2\pi)^2\delta^2(\vec{\ell}-\vec{\ell}')P_\Phi(|\vec{\ell}|)\delta(D_1'-D_1). \quad \text{(A11)}$$

Thus, for $z \le z'$ we have

$$\langle\tilde{\gamma}^*_{13}(\vec{\ell},z)\tilde{\gamma}_{13}(\vec{\ell}',z')\rangle = \frac{4}{D(z)D(z')}\ell_1\ell_1'(2\pi)^2\delta^2(\vec{\ell}-\vec{\ell}')\int_0^{D(z)} dD_1 P_\Phi(\ell), \quad \text{(A12)}$$

where $l \equiv |\vec{\ell}|$ and $P_\Phi(\ell)$ is the angular power spectrum,

$$P_\Phi(\ell) = \frac{P_\Phi(k=\ell/D_1)}{D_1^2} = \left[\frac{3}{2}\Omega_m H_0^2(1+z_1)\right]^2\frac{P_\delta(k,z_1)}{k^4 D_1^2}, \quad \text{(A13)}$$

where P_δ is the matter power spectrum.

If we define the power spectrum $P_{13}(\vec{\ell},z,z')$ of γ_{13} components as

$$\langle\tilde{\gamma}^*_{13}(\vec{\ell},z)\tilde{\gamma}_{13}(\vec{\ell}',z')\rangle \equiv (2\pi)^2 P_{13}(\vec{\ell},z,z')\delta^2(\vec{\ell}-\vec{\ell}'), \quad \text{(A14)}$$

then we have

$$P_{13}(\vec{\ell},z,z') = \frac{4\ell_1^2}{D(z)D(z')}\int_0^{D(z)} dD_1 P_\Phi(\ell). \quad \text{(A15)}$$

There are similar results for the power spectrum P_{23} of γ_{23} component. Furthermore, we can define the transverse power spectrum P_t as follows,

$$P_t(\ell,z,z') \equiv P_{13}+P_{23} = \frac{4l^2}{D(z)D(z')}\int_0^{D(z)} dD_1 P_\Phi(\ell). \quad \text{(A16)}$$

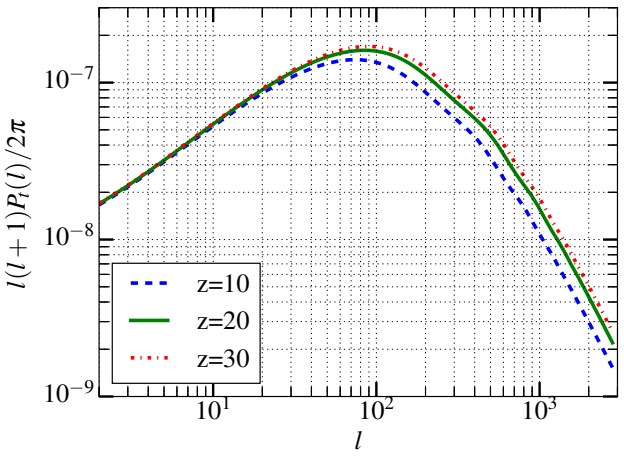

Figure 8. The transverse power spectra for sources at redshifts $z = 10$(bottom), 20 and 30(top), predicted for the WMAP 7-year best fit cosmology ($\Omega_m = 0.265, \sigma_8 = 0.8, H_0 = 71.9$ km s^{-1}Mpc^{-1}).

This transverse power spectrum does not depend on the components but the magnitude of the angular wave number vector.

If the separation between z and z' are negligible, i.e. $z = z'$, we have

$$P_t(\ell,z) = \frac{4l^2}{D^2(z)}\int_0^{D(z)} dD_1 P_\Phi(\ell). \quad \text{(A17)}$$

The results are shown in Fig.8.

2. Lensing Contamination

Ref. [**?**] has found the expression of the brightness temperature fluctuation δT_b as a function of the magnitude of magnetic fields, i.e. Eq. (**??**). To make the derivation concise, we define several quantities as below.

$$\bar{x}_{\rm B} \equiv \frac{x_{\rm B}}{B} = \frac{g_e\mu_{\rm B}T_*}{2\hbar A T_\gamma}, \quad \text{(A18)}$$

$$A \equiv \left(1-\frac{T_\gamma}{T_{\rm s}}\right)x_{1{\rm s}}\left(\frac{1+z}{10}\right)^{1/2}, \quad \text{(A19)}$$

$$C \equiv 0.128\ {\rm mK}\left(\frac{T_\gamma}{T_{\rm s}}\right)x_{1{\rm s}}\left(\frac{1+z}{10}\right)^{1/2}, \quad \text{(A20)}$$

$$\mu \equiv \frac{C}{10}\frac{x_B}{(1+x_{\alpha,(2)}+x_{c,(2)})^2}, \quad \text{(A21)}$$

$$\lambda \equiv 13.2 - C - \frac{C}{20}\frac{1}{1+x_{\alpha,(2)}+x_{c,(2)}}, \quad \text{(A22)}$$

$$q \equiv 39.6 - 3C - \frac{C}{60}\frac{1}{1+x_{\alpha,(2)}+x_{c,(2)}}. \quad \text{(A23)}$$

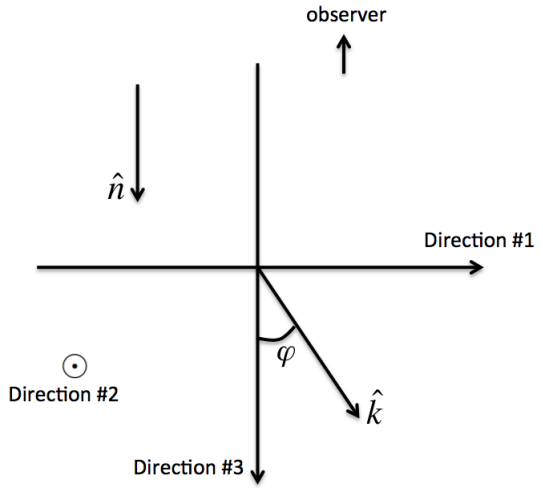

Figure 9. The coordinate system

The power spectrum of the brightness temperature is related to the matter power spectrum $P_\delta(k)$ by

$$P_{T_b}(\boldsymbol{k}) = \left|\frac{\partial\delta T_b}{\partial\delta}\right|^2 P_\delta(k). \tag{A24}$$

The transfer function $\partial\delta T_b/\partial\delta$ is given by taking derivative of Eq. (**??**), i.e.

$$\frac{\partial\delta T_b}{\partial\delta} = A\left[(26.4-2C)\left(1+(\hat{\boldsymbol{k}}\cdot\hat{\boldsymbol{n}})^2\right) - \frac{C}{15}\sum_m \frac{4\pi}{5}\frac{Y_{2m}(\hat{\boldsymbol{k}})[Y_{2m}(\hat{\boldsymbol{n}})]^*}{1+x_{\alpha,(2)}+x_{c,(2)}-imx_B}\right] \tag{A25}$$

By expanding Eqn.(A25) for small magnetic field B (small x_B), we will obtain a precession correction on the original P_{T_b} profile. The tangent of the precession angle θ_{pr} is proportional to the magnitude of the magnetic field applied.

To see that, let's first define our coordinate system as shown in Fig.9. The unit vectors then will be $\hat{k} = (\pi/2, \varphi)$ and $\hat{n} = (\pi/2, 0)$, where the first coordinate represents the angle between the Direction #2 and the vector. The expansion becomes

$$\frac{\partial\delta T_b}{\partial\delta} = A(q + \lambda\cos 2\varphi + \mu\sin 2\varphi). \tag{A26}$$

Due to the $\sin 2\varphi$ term contributed by the small magnetic field, the original profile gets a small precession angle θ_{pr}

$$\theta_{pr} \simeq \tan\theta_{pr} = -\frac{\mu}{\lambda}, \tag{A27}$$

Thus, if we measure the precession angle θ_{pr} in the power spectra of T_b, we can determine the magnitude of the magnetic field.

Next we will show that the transverse components of the weak lensing can also produce a similar precession angle.

In the 3D Cartesian coordinate, the unit vectors are written as

$$\hat{k} = (\sin\varphi, 0, \cos\varphi),\ \hat{n} = (0,0,1), \tag{A28}$$

and they are distorted into

$$\hat{k}' = \begin{pmatrix} (1+\kappa+\gamma_{11})\sin\varphi + \gamma_{13}\cos\varphi \\ \gamma_{12}\sin\varphi + \gamma_{23}\cos\varphi \\ \gamma_{13}\sin\varphi + (1+\kappa+\gamma_{33})\cos\varphi \end{pmatrix},$$
$$\hat{n}' = (\gamma_{13}, \gamma_{23}, 1+\kappa+\gamma_{33}). \tag{A29}$$

Since the shearing components are all very small, by taking the first order, we obtain the shear only change φ by

$$\Delta\varphi \simeq \sin\Delta\varphi \simeq -2\gamma_{13}. \tag{A30}$$

Thus, if there is no magnetic field ($x_B = 0$), due to the weak lensing, the transfer function (A26) will become

$$\frac{\partial\delta T_b}{\partial\delta} = A[q + \lambda(\cos 2\varphi + 4\gamma_{13}\sin 2\varphi)]. \tag{A31}$$

Since the weak lensing also spurs the k in $P_\delta(k)$, we need to find the relation between $P_\delta(k')$ and $P_\delta(k)$. To the first order, we can find

$$k' = k(1+\kappa+\gamma_{11}\sin^2\varphi + \gamma_{33}\cos^2\varphi + 2\gamma_{13}\sin\varphi\cos\varphi). \tag{A32}$$

Since $P_\delta(k) \propto k^{n_{\rm eff}}$, we have

$$P_{T_b}(\vec{k}') = \left|\frac{\partial\delta T_b}{\partial\delta}[1+\kappa+\gamma_{11}\sin^2\varphi + \gamma_{33}\cos^2\varphi + 2\gamma_{13}\sin\varphi\cos\varphi]^{n_{\rm eff}/2}]\right|^2 P_\delta(k), \tag{A33}$$

where $n_{\rm eff}$ is the effective spectral index. We can see all the quadropole features in the power spectra of T_b come from the modified transfer function.

After expanding, keeping the first-order terms and neglecting small octupole terms, we can obtain the modified transfer function, and find the precession angle again, given by the negative ratio of the two coefficients of the quadrupole terms,

$$\theta'_{pr} \simeq -\left(4 + \frac{n_{\rm eff}}{2}\frac{q}{\lambda}\right)\gamma_{13}. \tag{A34}$$

This precession angle is made by the transverse weak lensing component instead of the magnetic field, but the effect it makes looks like there is a (fake) magnetic field such that

$$\frac{\mu}{\lambda} = \left(4 + \frac{n_{\rm eff}}{2}\frac{q}{\lambda}\right)\gamma_{13}, \tag{A35}$$

where we can solve for the (fake) comoving magnetic field

$$B_{\rm lensing,13} = \frac{10(1+x_{\alpha,(2)}+x_{c,(2)})^2(4\lambda + \frac{n_{\rm eff}}{2}q)}{C\bar{x}_{\rm B}(1+z)^2}\gamma_{13} \equiv \alpha\gamma_{13}. \tag{A36}$$

Finally, we find the power spectrum of the comoving lensing magnetic field

$$P_B^{\rm lensing,13}(\ell) = \left|\frac{\partial B_{\rm lensing,13}}{\partial \gamma_{13}}\right|^2 P_{\gamma_{13}}(\ell) = \alpha^2 P_{\gamma_{13}}(\ell). \tag{A37}$$

Note that this power spectrum is only the contribution from γ_{13} component because we assume $\hat{k}$ to sit on the "1-3" plane. For any position on the sky, one has the choice to rotate his coordinate system to maximize or minimize P_{13}. However, randomly, the total power spectrum of comoving lensing magnetic field picks up an average value, i.e. the half maximum,

$$P_B^{\rm lensing}(\ell) = \frac{\alpha^2}{2} P_t(\ell), \tag{A38}$$

$$\Delta_B^{\rm lensing}(\ell) = \sqrt{\frac{l(l+1)}{2\pi} P_B^{\rm lensing}(\ell)} \tag{A39}$$

For a survey with $\Omega_{\rm survey} = 1$sr, the scale of interest is about $l = 6$. The scale of matter fluctuations relavant to the observed signals is determined by the resolution of the inferometers as

$$k \sim \frac{2\pi L}{\lambda_0(1+z)D} \sim 1, \tag{A40}$$

corresponding to $n_{\rm eff} \sim -2.274$.

3. De-lensing

Here is the basic idea of de-lensing.

Consider we have a signal $\vec{x}$, expressed by random variables $x_1, x_2, \cdots, x_M$, so that when we measure the values of $x_1, x_2, \cdots, x_M$, we get variances $C_{11}, C_{22}, \cdots, C_{MM}$, as well as their covariances. Suppose we can detect another signal $\vec{y}$, expressed by random variables $y_1, y_2, \cdots, y_N$, with their variances and covariances, we can use them to further constrain the variances of measuring $\vec{x}$, if $\vec{x}$ and $\vec{y}$ are correlated.

In the simplest case, we assume $\vec{x}$, $\vec{y}$ are Gaussian random variables and $\vec{x}, \vec{y}$ obey the 2-dimensional Gaussian distribution. Then we can write the covariance matrix as

$$\mathbf{C} = \begin{pmatrix} \mathbf{C}^{xx} & \mathbf{C}^{xy} \\ \mathbf{C}^{yx} & \mathbf{C}^{yy} \end{pmatrix}, \tag{A41}$$

where $\mathbf{C}$ is a $(M+N)\times(M+N)$ matrix.

Now we can work out the probability of obtaining $\vec{x}$ given $\vec{y}$:

$$\begin{aligned} P(\vec{x}|\vec{y}) &= \frac{P(\vec{x},\vec{y})}{P(\vec{y})} \\ &= (2\pi)^{-M/2} (\det \mathbf{C}^{xx}_{post})^{-1/2} \exp\left\{ -\frac{1}{2}\left[\vec{x} + \left(\left(\mathbf{C}^{-1}\right)^{xx}\right)^{-1}\left(\mathbf{C}^{-1}\right)^{xy}\vec{y}\right]^T \left(\mathbf{C}^{xx}_{post}\right)^{-1}\left[\vec{x} + \left(\left(\mathbf{C}^{-1}\right)^{xx}\right)^{-1}\left(\mathbf{C}^{-1}\right)^{xy}\vec{y}\right]\right\}. \end{aligned} \tag{A42}$$

The last line shows that the posterior probability of obtaining signal $\vec{x}$ still satisfies a Gaussian distribution, with shifted mean values of $\vec{x}$ and a posterior covariance matrix $\mathbf{C}^{xx}_{post}$:

$$\begin{aligned} \det \mathbf{C}^{xx}_{post} &\equiv \frac{\det \mathbf{C}}{\det \mathbf{C}^{yy}}, \\ \langle \vec{x} \rangle|_{\vec{y}} &\equiv -\left(\left(\mathbf{C}^{-1}\right)^{xx}\right)^{-1}\left(\mathbf{C}^{-1}\right)^{xy}\vec{y}, \\ \left(\mathbf{C}^{xx}_{post}\right)^{-1} &= \left(\mathbf{C}^{-1}\right)^{xx}. \end{aligned} \tag{A43}$$

Finally we have this relation:

$$\mathbf{C}^{xx}_{post} = \left[\left(\mathbf{C}^{-1}\right)^{xx}\right]^{-1}. \tag{A44}$$

We can further apply the blockwise inversion formula to prove that by doing this, we can get a better constraint on $\vec{x}$ and lower the variance in $\mathbf{C}^{xx}$.

Now applying to the de-lensing case, γ_{13} is the signal we want to constrain, and CMB convergence κ is the additional signal provided. Going through a very similar derivation, we obtain the power spectrum of CMB convergence, as well as the cross spectra between transverse shear components and CMB convergence,

$$\begin{aligned} P_\kappa(\vec{\ell}) &= l^4 \int_0^{D_0} dD_1 \left(\frac{1}{D_1(z_1)} - \frac{1}{D_0}\right)^2 P_\Phi(\ell), \\ P_{13,\kappa}(\vec{\ell}, z_i) &= \frac{2i\ell_1 l^2}{D(z_i)} \int_0^{D(z_i)} dD_1 \left(\frac{1}{D_1(z_1)} - \frac{1}{D_0}\right) P_\Phi(\ell), \end{aligned} \tag{A45}$$

where D_0 is the comoving distance of the CMB.

For the N redshift slices and the angular scale l that we are interested in, we can write the covariance matrix

as a $(N+1)\times(N+1)$ matrix,

$$\mathbf{C}_l = \begin{pmatrix} \mathbf{P}^{13} & \mathbf{P}^{13,\kappa} \\ \mathbf{P}^{\kappa,13} & \mathbf{P}^{\kappa} \end{pmatrix}, \tag{A46}$$

where $\mathbf{P}^{13}$ is the $N\times N$ matrix formed by $P_{13}(\vec{\ell}, z_i, z_j)$, $\mathbf{P}^{13,\kappa}$ the $N\times 1$ matrix formed by $P_{13,\kappa}(\vec{\ell}, z_i)$, $\mathbf{P}^{\kappa}$ the number $P_{\kappa}(\vec{\ell})$. $\mathbf{P}^{\kappa,13}$ can be obtained by taking Hermitian conjugate of $\mathbf{P}^{13,\kappa}$.

After de-lensing, the posterior convariance matrix of $\mathbf{P}^{13}$ becomes

$$\mathbf{P}^{13}_{\rm post} = \left((\mathbf{C}_l^{-1})^{NN}\right)^{-1}, \tag{A47}$$

where $(\cdots)^{NN}$ means taking the upper left $N\times N$ submatrix. Note that this time we need to do the average over the choices of coordinate for the posterior power spectra instead of the prior ones. That means we set $\ell_1 = l$ at first, after calculating the posteriors, we average them over the choices of coordinate, which turns out to just introduce a factor of $1/2$ as previous.

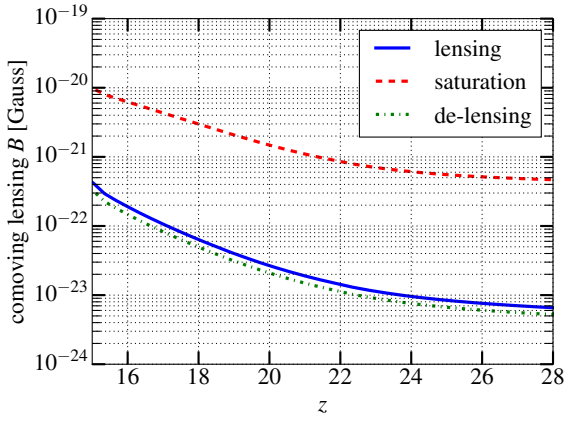

Figure 10. The 1σ comoving lensing magnetic field before and after de-lensing, as produced by the transverse shearing effect of weak lensing, compared to the saturation limit of our method.